Published in final edited form as:
Mamm Genome. 2011 April ; 22(3-4): 156–169. doi:10.1007/s00335-010-9309-z.

Molecular characterization of an allelic series of mutations in the mouse *Nox3* gene

John P. Flaherty, **Heather E. Fairfield**, **Catrina A. Spruce**, **Christopher M. McCarty**, and **David E. Bergstrom**
The Jackson Laboratory, 600 Main Street, Bar Harbor, ME 04609, USA

Abstract

The inner ear consists of the cochlea (the organ of hearing) and the vestibular system (the organs of balance). Within the vestibular system, linear acceleration and gravity are detected by the saccule and utricle. Resting above the neurosensory epithelia of these organs are otoconia, minute proteinaceous and crystalline (calcite) inertial masses that shift under the physical forces imparted by linear movements and gravity. It is the transduction and sensation of these movements and their integration with vision and proprioceptive inputs that contribute to the sensation of balance. It has been proposed that a reactive oxygen species- (ROS-) generating NADPH oxidase comprising the gene products of the *Nox3*, *Noxo1*, and *Cyba* genes plays a critical and constructive role in the process of inner-ear development, specifically, the deposition of otoconia. Inactivation in mouse of any of the NADPH oxidase components encoded by the *Nox3*, *Noxo1*, or *Cyba* gene results in the complete congenital absence of otoconia and profound vestibular dysfunction. Here we describe our use of PCR, reverse transcription-PCR (RT-PCR), and rapid amplification of cDNA ends (RACE) with traditional and high-throughput (HTP) sequencing technologies to extend and complete the molecular characterization of an allelic series of seven mutations in the *Nox3* gene. Collectively, the mutation spectrum includes an endogenous retrovirus insertion, two missense mutations, a splice donor mutation, a splice acceptor mutation, premature translational termination, and a small duplication. Together, these alleles provide tools to investigate the mechanisms of otoconial deposition over development, throughout aging, and in various disease states.

Introduction

The mouse *Nox3* gene encodes an NADPH oxidase that is expressed primarily in the inner ear and is known to be required for the proper development and function of the vestibular system (Banfi et al. 2004; Cheng et al. 2001; Paffenholz et al. 2004). Specifically, the six-transmembrane NADPH-binding protein encoded by *Nox3* is believed to interact with a two-transmembrane protein encoded by *Cyba* and a cytosolic protein encoded by *Noxo1* to form part, or all, of a functional NADPH oxidase complex that is capable of transporting electrons across biological membranes to oxygen (O_2) forming superoxide ($O_2^{\bullet -}$) and a cascade of subsequent reactive oxygen species (ROS).

Mutation of any of these three components has a profound effect on the ability of mice to detect linear acceleration or gravity, deficits manifested overtly by abnormalities in behavior

dave.bergstrom@jax.org .
Present Address: J. P. Flaherty New York College of Osteopathic Medicine of New York Institute of Technology, Northern Boulevard, P.O. Box 8000, Old Westbury, NY 11568, USA
Present Address: C. M. McCarty Mount Desert Island Biological Laboratory, Old Bar Harbor Road, Salisbury Cove, ME 04672, USA

(Bergstrom et al. 2004; Kiss et al. 2006; Nakano et al. 2008; Paffenholz et al. 2004). Aberrant behavior may include oblique posturing of the head and, to varying degrees, hyperactivity and circling. Additional behavioral abnormalities are apparent when the animals are challenged and include impaired air and ground righting reflexes, poor performance on rotating rod and stationary balance beam tests, and an inability to swim.

Although the saccule and utricle (the linear acceleration-and gravity-detecting organs within the vestibule) exhibit no apparent cellular abnormalities, in mutant mice they nonetheless remain inactive due to a complete congenital absence of otoconia, crystalline inertial masses that normally rest atop these organs (Jones et al. 1999; Nakano et al. 2008). In normal mice, in response to physical forces, the otoconia shift imparting shearing forces on the underlying stereocilia of the saccule and utricle. These mechanical signals are transduced by the saccule and utricle into action potentials that propagate along the eighth cranial (vestibulocochlear, VIII) nerve to the brain.

Jones et al. have developed a noninvasive method for detecting these vestibular-evoked potentials (VsEPs) (Jones and Jones 1999; Jones et al. 1999, 2002, 2003a, b, 2004, 2004, 2006), and it has now been shown that homozygosity for loss-of-function mutations in each of *Nox3*, *Cyba*, and *Noxo1* leads to the complete loss of VsEPs (Jones et al. 1999; Nakano et al. 2008). Thus, it seems quite clear that the production of ROS plays an important and constructive role in the development and function of the vestibular system.

In the cochlea, the organ of hearing, the situation may be quite the opposite. Due to their reactive nature, ROS interact with a variety of small inorganic molecules and biological macromolecules and can cause irreversible oxidative damage to these targets specifically, as well as to cells and organisms more generally (Bedard and Krause 2007). In fact, ROS have been widely implicated as factors in age-, noise-, and drug-induced hearing loss (Darrat et al. 2007; Guthrie 2008; Henderson et al. 1999, 2006; Hosokawa 2002; Kopke et al. 1999; Rybak et al. 2007; van den Berg et al. 2006). Moreover, the discovery of *Nox3* in the inner ear has raised the possibility of the *Nox3*-dependent NADPH oxidase as a source of potentially harmful ROS in these settings. A recent study by Mukherjea et al. (2010) suggests that this may indeed be the case. In their study, the authors were able to inhibit cisplatin-induced hearing loss in the chinchilla by the transtympanic administration of a siRNA directed against *Nox3*. In other studies the complete loss of function at the *Nox3* locus may provide protection against hearing loss in some susceptible strains (K.N. Mills and S.M. Jones, personal communication). Accordingly, whether it be to understand a constructive role in the structure and function of the vestibular system, or possible deleterious roles in age-, noise-, and drug-related hearing loss, a complete understanding of the function of inner-ear NADPH oxidase components and their mutant alleles is required.

Studies of such allelic series (e.g., *Lmna* and associated laminopathies, for reviews see Burke and Stewart 2006; Capell and Collins 2006; Scharner et al. 2010; Stewart et al. 2007; Worman et al. 2009) are informative by identifying structure/function relationships across the various domains of multidomain proteins and by displaying the broad range of phenotypic consequences potentially engendered by a wide spectrum of mutation types and locations. Moreover, by identifying mutant alleles with various characters (hypermorphic, hypomorphic, neomorphic, antimorphic), the geneticist is often empowered to conduct a detailed functional dissection of mechanism. In addition, when mutant alleles arise spontaneously on strains not commonly employed in large gene-trapping and gene-targeting projects, mutant phenotypes can be altered by genetic modifiers present in the novel strain. This provides deeper insight into the role that genetic background can have on the manifestation of phenotype, can lead to the identification of modifying genes, and offers inroads to other interacting factors and pathways.

In regard to alleles of the inner-ear NADPH oxidase, a full molecular characterization of mutation types may prove necessary for understanding the range of clinical presentation among patients at vestibular testing facilities and the range of phenotypes observed among mutation-bearing strain sets in the basic sciences laboratory. In this regard, a survey of the Mouse Genome Informatics website identifies mutant mouse strains representing a single mutant allele of *Noxo1* (known as *hslt*), a single mutant allele of Cyba (known as *nmf333*) and six mutant alleles of *Nox3* (known as *het*, *het-2J*, *het-3J*, *het-4J*, *R96*, and *R542*) (Bergstrom et al. 2004; Kiss et al. 2006; Nakano et al. 2008; Paffenholz et al. 2004). With the addition of a newly identified allele of *Nox3* (*het-5J*) described in this report, the number of *Nox3* mutant alleles represented by mouse strains is now seven.

In this study we describe our use of PCR, reverse transcription-PCR (RT-PCR), and rapid amplification of cDNA ends (RACE), as well as traditional Sanger sequencing methods and more recent high-throughput (HTP) sequencing technologies, to extend and complete the molecular characterization of all of the known mutant alleles at *Nox3*. In turn, we hope to gain a greater understanding of the genotype/phenotype correlations in *Nox3* function and the important roles *Nox3* plays in development, physiology and disease.

Materials and methods

Mice

All mice were obtained from The Jackson Laboratory (Bar Harbor, ME) and were housed on a bedding of white pine shavings and fed NIH-31 5K54 (4% fat) or NIH-31 5K52 (6% fat) diet and acidified water *ad libitum*. All experiments were performed with the approval of The Jackson Laboratory Institutional Animal Care and Use Committee (IACUC) and in compliance with all applicable laws and guidelines.

Nomenclature

All mouse alleles, genes, and strains are referred to by official nomenclature. The *Nox3*^{het} allele arose spontaneously on the GL/Le strain (JAX #000255) but has since been made congenic (#002557) onto the C57BL/6JEiJ strain (#000924). The *Nox3*$^{het–2J}$ allele arose spontaneously on the B10.D1-*H2*^{q}/SgJ strain (#002024) and has been cryopreserved as an F1 hybrid (#003483) with the C57BL/6J strain (#000664). The *Nox3*$^{het–3J}$ allele arose during ethyl methane sulfonate- (EMS-) induced mutagenesis of CJ7 ES cells (strain 129S1/SvImJ, #002448) and has since been made congenic onto the C57BL/6J strain (#000664). The *Nox3*$^{het–4J}$ allele (#005014) arose during *N*-ethyl-*N*-nitrosourea- (ENU-) induced mutagenesis of C57BL/6J mice (#000664). The *Nox3*$^{het–5J}$ allele arose spontaneously on the CBySmn.CB17-*Prkdc*$^{scid/J}$ strain (#001803) but has since been crossed to the BALB/cByJ strain (#001026). Two remaining mutant alleles, the *Nox3*^{R542} and *Nox3*^{R96} alleles, arose during ENU-induced mutagenesis of the C3HeB/FeJ strain (#000658) but were not used in this study. Genomic coordinates are those from Build 37 of the mouse genome sequence. The numbering of the 13 exons of *Nox3* is according to the UCSC gene prediction in the mouse reference genome sequence (NCBI37/mm9) and differs from that shown in Fig. 4 of Paffenholz et al. (2004) by the addition of a single exon between exons 4 and 5, and the renumbering of all following exons.

Oligonucleotides

Oligonucleotides (Integrated DNA Technologies, Coralville, IA) used for genotyping, amplification of *Nox3* sequences from genomic DNA, RACE, or RT-PCR analysis of *Nox3* cDNAs are given in Table 1. Oligonucleotides were designed using the Primer 3.0 algorithm alone (Rozen and Skaletsky 2000) or in conjunction with the ExonPrimer function (Institute

of Human Genetics, Helmholtz Center Munich, Munich, Germany) of the UCSC Genome Browser (Kent et al. 2002).

PCR

Unless otherwise stated, all PCR reactions were performed using the following cycling conditions: preheating at 95°C for 3 min; 40 cycles of amplification at 95°C for 30 s, 55°C for 30 s, and 72°C for 30 s; and a final extension of 72°C for 9 min 30 s.

RT-PCR

Total RNA was isolated from individual adult wild-type, heterozygous, and homozygous mutant temporal bone explants (containing the inner ear) using an RNeasy Mini Kit (Qiagen, Valencia, CA) according to the manufacturer's directions. First-strand synthesis reactions (generally 8 μl RNA, 200–300 ng) were run in accordance with the SuperScript III (Invitrogen, Carlsbad, CA) random hexamer or similar protocols. PCR reactions (30 μl) were performed on cDNA and on no-reverse transcriptase controls to amplify segments of the *Nox3* transcript. Each reaction used 2 μl cDNA, 5 Prime Master Mix (5 Prime, Gaithersburg, MD; final concentration 1X), and the appropriate primers (200 nM) or similar reaction conditions. Amplification was performed on a MJ Research (Waltham, MA) PTC-200 Thermocycler (Bio-Rad, Hercules, CA) and involved a 2:30-min denaturing step at 95°C followed by 40 cycles at 95°C for 30 s, 55°C for 30 s, and a 72°C extension step for 90 s. Products were resolved on 1–2% SeaKem LE agarose gels (Lonza, Basel, Switzerland).

RACE

Total RNA was isolated from individual adult wild-type, heterozygous, and homozygous mutant temporal bone explants (containing the inner ear) using an RNeasy Mini Kit (Qiagen) according to the manufacturer's directions. RACE reactions were performed using a First Choice RLM-RACE Kit (Ambion, Austin, TX) according to the manufacturer's directions. Products were resolved on 1–2% SeaKem LE agarose gels (Lonza).

Sequencing

Sanger sequencing—Amplification products were purified using a Qiagen QIAquick or a MinElute PCR Purification Kit according to manufacturer's directions. Cycle sequencing reactions were performed on PCR products (5–20-ng product, 20 pmol sequencing primer) using the ABI BigDye Terminator Chemistry v3.1 (Applied Biosystems, Carlsbad, CA). Finished reactions were purified using the Agencourt CleanSeq system (Agencourt, Bioscience Corp., Beverly, MA) and resolved on an ABI 3730xl DNA sequencer. Sequence reads were analyzed and aligned using Sequencher software (Gene Codes Corp., Ann Arbor, MI).

Next-generation sequencing—Sequencing libraries (v4, Illumina, Inc., San Diego, CA) were prepared from B6Ei.GL-*Nox3*^{het}/*Nox3*^{het} and B6.129S1-*Nox3*$^{het–3J}$/*Nox3*$^{het–3J}$ DNA, bar-coded, and hybridized to a sequence capture array (Agilent, Inc., Santa Clara, CA) containing 358,713 probes (3-bp offset) arrayed in duplicate and designed from unique Chromosome 17 sequences in and around *Nox3* (Chr 17: nt 3367120–5220663). Eluted DNA was sequenced by the 75-nucleotide paired-end method using an Illumina GAIIx Genome Analyzer. Sequence reads were downloaded and then processed and mapped to the C57BL/6J (Build 37) reference sequence using the Burrows–Wheeler Aligner (Li and Durbin 2010). Sequences were then viewed graphically using the Integrative Genomics Viewer (IGV, Broad Institute, Cambridge, MA).

Observation of otoconia in cleared temporal bones

Temporal bones were dissected from euthanized adult mice. Specimens were fixed by flushing neutral buffered formalin through a hole in the cochlear apex prior to immersion in neutral buffered formalin for 1–12 h. Specimens were then briefly washed and dehydrated through hourly or overnight washes in an ascending ethanol series (70–100%). Finally, specimens were cleared overnight in methyl salicylate and observed/photographed under polarized light on a dissecting microscope.

Results

The *Nox3^{het}* allele

The *Nox3^{het}* allele arose on the GL/Le strain of mice in 1976 (Sweet 1980) and has since been made congenic onto the C57BL/6JEiJ strain. We conducted RT-PCR and RACE analyses of total RNA purified from adult temporal bone/inner-ear explants from B6Ei.GL-*Nox3^{het}/Nox3^{het}* mice. Amplification products from the 5′ and central regions of the mutant cDNA were of sizes consistent with those expected from the predicted intron/exon structure of the *Nox3* gene. In contrast, however, 3′ RACE amplification products from exon 10 to the 3′ end of the mutant cDNA were not only the expected size of 600 bp, but also the unexpected sizes of approximately 400, 500, and 900 bp (Fig. 1). Purification and sequencing of the mutant amplification products revealed aberrant splicing causing three phenomena—the skipping of exons 11 and 12, the normal inclusion of exons 11 and 12, and the normal inclusion of exons 11 and 12 along with a cryptic exon downstream of exon 12—but in all cases invariably splicing into a novel (not *Nox3*-derived) terminal sequence prior to exon 13. The results of a BLAST search of the short terminal sequence most closely matched database entries representing the family of mouse endogenous retroviral elements (ERVs); however, due to the small size of the insertion captured within the mutant cDNA, a definitive identification was not possible. From these results we hypothesized that a retroviral element had inserted into intron 12 and that a portion of the retroviral sequence was being inappropriately spliced into *Nox3* mRNAs. To test this hypothesis we set up a series of amplification reactions across intron 12 of the *Nox3* gene using both C57BL/6JEiJ and B6Ei.GL-*Nox3^{het}/Nox3^{het}* genomic DNAs as the amplification template. All segments of intron 12 amplified as expected from control DNA. In contrast, for mutant DNA, two overlapping regions failed to amplify, suggesting an insertion in mutant DNA within the 61-bp region of overlap. Long PCR reactions designed to span the putative insertion failed, suggesting an insertion of several kilobases or more, or otherwise resistant to amplification. To further substantiate these findings and obtain sequence from within the putative insertion, we took a sequence-by-synthesis approach. Sequencing libraries were prepared from B6Ei.GL-*Nox3^{het}/Nox3^{het}* DNA and hybridized to a sequence capture array designed from 1,185,475 bp of unique Chromosome 17 sequences (representing 64.0% of the overall 1,853,543-bp region) in and around *Nox3*. Eluted DNA was sequenced using an Illumina GAIIx Genome Analyzer. Sequence reads were downloaded and then processed and mapped to the C57BL/6J (mm9) reference sequence using the Burrows–Wheeler Aligner (Li and Durbin 2010). Analysis showed that 99.73% of the probed sequences were covered by the *Nox3^{het}* sequence data. Sequences were then viewed graphically using the Integrative Genome Viewer.

Within the immediate region of the suspected insertion, several interesting features were apparent on the IGV display (Fig. 2). First, several reads within the area of the insertion were denoted as having paired ends that mapped to a chromosome other than Chromosome 17. Next, while most reads outside of the area of the suspected insertion were generally of uniform length and offset from each other by one or a few nucleotides on each end, those in the immediate area of the suspected insertion appeared truncated by varying lengths such

that many of the reads aligned at their truncated ends. Reads leading from the area of the suspected insertion toward the proximal end of the chromosome and those leading toward the distal end overlapped by a 7-nt sequence (ACATATA). We reasoned that sequence reads overlapping the insertion site at each end were truncated by the sequence-processing algorithm to eliminate portions of the read derived from insertion sequences not present in the reference genome. With regard to distally pointing reads, this process seemed imperfect, leaving a few nucleotides of poorly aligning sequence still present on the otherwise truncated read. To further analyze the region, we obtained all sequence reads that mapped completely or at least on one end to this area of Chromosome 17. The sequences were then used to construct local alignments de novo. When aligned, two interesting contigs emerged (shown in part in Fig. 3a). One contig consisted of sequences immediately proximal to the area of the suspected insertion; next, contained a 7-nt TATATGT sequence, i.e., the reverse complement of the ACATATA sequence of read overlap observed in the IGV display; and, finally, ended with a sequence that when analyzed by the CENSOR function of the GIRI REPBASE Update (Jurka et al. 2005) showed strong similarity to the mouse endogenous retrovirus class 13B (similarity score = 0.8161, BLAST alignment score = 502). Likewise, the second contig consisted of sequences immediately distal to the area of the suspected insertion; again, contained the 7-nt TATATGT sequence of read overlap observed in the IGV display; and, finally, ended with a sequence that showed strong similarity to the mouse endogenous retrovirus class 13A2 (similarity score = 0.8651, BLAST alignment score = 814). The results of the RACE, PCR, and HTP sequencing analyses are entirely consistent with the insertion of an ERV element immediately after nucleotide 3643197 of Chromosome 17 and causing a 7-nt target site duplication of nucleotides 3643191–3643197. It is this sequence that is present within both of the local alignment contigs and displayed as a region of overlap in the IGV display. Furthermore, mapping the insertion point among the intron 12 amplicons easily explains the basis of the two failed assays, as the integration site of the ERV interrupts the 3′ more (chromosome-proximal) assay and disrupts one of the primer binding sites of the 5′ more (chromosome-distal) assay.

Using this new knowledge of the *Nox3*^{het} causative mutation, we designed a direct PCR assay for the *Nox3*^{het} allele by selecting a pair of PCR primers that flank and a third primer within the ERV insertion (Fig. 3b). This assay clearly distinguishes among *Nox3*^{het}/*Nox3*^{het}, *Nox3*^{het}/+, and +/+ genotypes.

The *Nox3*$^{het–3J}$ allele

The *Nox3*$^{het–3J}$ allele arose as part of an ethyl methane sulfonate (EMS) mutagenesis project of CJ7 embryonic stem cells (Munroe et al. 2000) and has been shown to be allelic to *Nox3* by complementation test (Paffenholz et al. 2004). Although capable of producing a variety of mutation types, EMS most often results in guanine-to-adenine transitions (Klungland et al. 1995; Munroe et al. 2000). We prepared sequencing libraries from B6.129-*Nox3*$^{het–3J}$/*Nox3*$^{het–3J}$ mutant DNA, captured regions of DNA in and around *Nox3* using the same custom capture array described above, and sequenced the DNA using an Illumina GAIIx Genome Analyzer. Analysis showed that 99.73% of the probed sequences were covered by the *Nox3*$^{het–3J}$ sequence data. Sequence data were uploaded to the Computational Sciences Statistics and Analysis Group of The Jackson Laboratory and compared to C57BL/6J reference sequence, resulting in an annotation file of nearly 6000 lines of annotated differences from reference. Most variants appeared at extremely low allele frequencies and were interpreted as spurious sequencing artifacts. Of the remaining variants, comparison to mouse genomic sequence of inbred strains (Wellcome Trust Sanger Institute, Hinxton, UK) revealed that most of the sequence variants represented single nucleotide polymorphisms (SNPs) within the 129S1/SvImJ-derived congenic region surrounding the *het-3J* allele. One variant, however, was observed within the highly conserved splice acceptor site at the 3′ end

of intron 1 that was not present in 129S1/SvImJ genomic sequence (Chromosome 17, position 3695584). This sequence variant was confirmed by the Sanger dideoxy method (Fig. 4a). RT-PCR analysis clearly demonstrates the effect this mutation has on *Nox3* splicing (Fig. 4b). Although splicing of adult temporal bone/inner-ear RNA in wild-type (+/+) C57BL/6J mice is as expected, in B6.129-*Nox3*$^{het\text{-}3J}$/*Nox3*$^{het–3J}$ homozygotes a sequenced 362-bp RT-PCR product amplified with exon 1 (forward) and exon 2 (reverse) primers demonstrates the use of a cryptic splice acceptor in intron 1 (Fig. 4b, left panel). When assessed with exon 1 (forward) and exon 4 (reverse) primers, the predominant RT-PCR product is consistent in size with transcripts omitting exon 2 (Fig. 4b, right panel). These models are shown schematically in Fig. 4c. The predicted effects on the NOX3 protein are the introduction of six novel amino acids prior to a premature stop codon, and deletion of amino acids 37–68 with the remainder of the protein remaining in frame. Also of note, the mutation, a guanine-to-adenine transition, is entirely consistent with the mutagenic profile typical of EMS. Combined, the complementation test, HTP sequencing, Sanger sequencing, and RT-PCR analysis clearly demonstrate that a guanine-to-adenine transition on Chromosome 17 at position 3695584 is the causative mutation underlying the vestibular dysfunction observed in *Nox3*$^{het\text{-}3J}$/*Nox3*$^{het–3J}$ mice.

The *Nox3*$^{het–4J}$ allele

The *Nox3*$^{het–4J}$ allele (also known as *nmf250*) arose as part of an *N*-ethyl-*N*-nitrosourea (ENU) mutagenesis program of C57BL/6J mice (Goldowitz et al. 2004). Complementation tests between *nmf250* mice and *Nox3*^{het} mice confirm that *nmf250* is allelic with *Nox3*. Thus, the *nmf250* allele has been redesignated as *het-4J*. We looked for the mutation underlying the *Nox3*$^{het–4J}$ allele by amplification and Sanger-based sequence analysis of genomic DNA in and around *Nox3* exons, that was amplified with paired primers positioned within flanking intronic sequence. The results of this analysis uncovered a thymine-to-adenine transversion at position 2 of the highly conserved splice donor sequence immediately following exon 10 (Chromosome 17, position 3665819, Fig. 5a). RT-PCR analysis of total RNA from adult temporal bone/inner-ear explants confirms aberrant splicing of *Nox3* transcripts in the mutant strain (consistent with omission of exon 10 and a resulting frameshift) that is not seen in wild-type control mice (Fig. 5b, c). Together, the complementation test, Sanger sequencing, and RT-PCR analysis clearly demonstrate that a thymine-to-adenine transversion on Chromosome 17 at position 3665819 is the causative mutation underlying the vestibular dysfunction observed in *Nox3*$^{het–4J}$/*Nox3*$^{het–4J}$ mice.

The *Nox3*$^{het–5J}$ allele

The *Nox3*$^{het–5J}$ allele (Fig. 6) arose spontaneously on the CBySmn.CB17-*Prkdc*^{scid}/J strain at The Jackson Laboratory, where it was identified by the Phenodeviant Search Program of the laboratory's Mouse Mutant Resource (Mouse Mutant Resource Web Site 2010). It has since been maintained by crossing to BALB/cByJ mice. Allelism with *Nox3* was confirmed by complementation test. To explore the molecular basis of the *Nox3*$^{het–5J}$ mutation, we conducted an RT-PCR analysis of total RNA purified from adult temporal bone/inner-ear explants from both *Nox3*$^{het–5J}$/*Nox3*$^{het–5J}$ homozygotes and BALB/cByJ control mice. Amplification products from the wild-type cDNA and most regions of the mutant cDNA were of sizes consistent with those expected from the predicted intron/ exon structure of the *Nox3* gene. In contrast, however, one RT-PCR amplification product from the 3′ region of mutant cDNA was of an unexpected size, approximately 150 bp larger than the wild-type product. Purification and sequencing of the mutant amplification product revealed a tandem duplication of exon 11 (Fig. 6a), suggesting a similar duplication of genomic DNA in and around the region of the duplicated exon (Fig. 6b, c). To test this hypothesis, we designed a series of upstream-pointing PCR primers within intron 10 (e.g., red and blue primers in Fig. 6b) and a series of downstream-pointing primers in intron 11 (e.g., green primer in Fig. 6b),

reasoning that in the event of a duplication encompassing exon 11, some of these otherwise divergently pointing primers would now be pointed toward each other (Fig. 6c) and of small enough size for amplification. Amplification reactions with mutant template DNA consisting of the forward primer in conjunction with each of the two reverse primers did result in strong amplification from each reaction that was not observed in the corresponding BALB/cByJ (+/+) control reaction (e.g., Fig. 6d). Purification and sequencing of the mutant amplification products allowed us to determine the extent of the tandem duplication on Chromosome 17 from position 3649673 to 3651846. Together, these results demonstrate that a 2173-bp tandem duplication on Chromosome 17 is the molecular lesion underlying the *Nox3*$^{het–5J}$ mutant allele. It should also be noted that the duplication of exon 11 (147 bp) in *Nox3* RNA is not predicted to result in a frameshift but, instead, to encode the duplication of 49 in-frame amino acids (amino acids 457–505) prior the translation of exons 12 and 13 and translational termination at the native stop codon.

Discussion

Allelic series are important for identifying structure/function relationships within proteins, for displaying the phenotypic consequences of specific mutations, and for identifying mutant alleles with various characteristics (e.g., hypermorphic, antimorphic). In addition, mutant alleles arising in various inbred strains provide insight into the phenotypic effects of genetic background and can lead to the identification of modifying genes and interacting pathways. In this report we considered the single mutant alleles of *Cyba* and *Noxo1* and extended previous studies to provide a complete molecular characterization of the seven known mutant alleles of the NADPH oxidase *Nox3* (Table 2, Fig. 7). In this section we discuss the effects of inactivating mutations, in-frame insertions/deletions, and missense mutations on NOX3 protein structure and function. A fuller understanding of *Nox3* mutant alleles may offer clues into the precise function of *Nox3* in the mammalian inner ear.

Inactivating mutations

Our interest in NADPH oxidase components is related to their primary role in otoconial deposition and, subsequently, the requirement for otoconia in the transduction of the mechanical shearing forces of linear acceleration into action potentials transmitted along the vestibulocochlear nerve. Thus, the presence/absence of otoconia and VsEPs can provide anatomical and physiological correlates of protein function. With regard to VsEPs, *Nox3*^{het} and *Nox3*$^{het–4J}$ homozygotes have been assessed, with both showing a complete absence of response (Jones et al. 1999; K.N. Mills and S.M. Jones, personal communication). Moreover, it has been described that these strains as well as *Nox3*^{R96} and *Noxo1*^{hslt} homozygotes exhibit a complete absence of otoconia (Bergstrom et al. 2004; Kiss et al. 2006; Paffenholz et al. 2004). In addition, the frameshift mutation in the *Noxo1*^{hslt} allele and the aberrant splicing in the *Nox3*^{het}, *Nox3*$^{het–3J}$, and *Nox3*$^{het–4J}$ alleles are predicted to lead to the introduction of premature stop codons. In sum, it is likely that *Nox3*^{het}, *Nox3*$^{het–3J}$, *Nox3*$^{het–4J}$, *Nox3*^{R96}, and *Noxo1*^{hslt} are all functional null alleles.

In-frame insertions/deletions

In addition to those alleles and splice forms leading to the premature termination of translation, the *Nox3*$^{het–5J}$ allele and at least one splice form of the *Nox3*$^{het–3J}$ allele have the potential to significantly alter NOX3 protein structure without altering the NOX3 reading frame. The aberrant *Nox3*$^{het–3J}$ transcript that omits exon 2 is predicted to result in an in-frame deletion of amino acids 37–67, including the first transmembrane domain. In vitro studies utilizing HEK (human embryonic kidney)-293 cells and CHO (Chinese hamster ovary)-K1 cells have highlighted key interactions among wild-type NOX3, CYBA, and NOXO1 proteins required for proper maturation and function of the *Nox3*-based NADPH

oxidase complex (Nakano et al. 2007), including interactions apart from the first transmembrane domain that may remain intact in the *Nox3*$^{het–3J}$ context. Likewise, the aberrant *Nox3*$^{het–5J}$ transcript that duplicates exon 11 is predicted to result in an in-frame duplication of amino acids 457–505, including a significant portion of the NADPH binding domain. Thus, while a case could be made for residual activity of the *Nox3*$^{het–3J}$ and *Nox3*$^{het–5J}$ alleles, no direct biochemical or physiological studies have investigated this possibility. Nonetheless, given the extensive alterations to the NOX3 protein, any physiologically significant activity seems unlikely. Indeed, the only measure of functional activity existing for the *Nox*$^{het–3J}$ and *Nox3*$^{het–5J}$ alleles, the assessment of otoconial density, suggests no functional activity as otoconia are consistently absent in Nox3$^{het–3J}$ and Nox3$^{het–5J}$ homozygotes.

Missense mutations

In addition to the protein-truncating mutations and extensive in-frame protein alterations described above, three mutant alleles of inner-ear NADPH oxidase components encode single-amino-acid missense mutations.

The *Nox3*$^{het–2J}$ allele encodes a nonconservative glycine-to-arginine (Gly > Arg) substitution of amino acid 428 of the NOX3 protein (Paffenholz et al. 2004; D. Bergstrom, unpublished results). Likewise, the *Nox3*^{R542} allele encodes a nonconservative lysine-to-glutamic acid (Lys > Glu) substitution of amino acid 526 of the NOX3 protein. Although no functional studies have been conducted with the *Nox3*^{R542} allele, recently electrophysiological studies have been conducted comparing the *Nox3*$^{het–2J}$ allele with the original *Nox3*^{het} allele (K.N. Mills and S.M. Jones, personal communication). In these studies, *Nox3*^{het}/+, *Nox3*$^{het–2J}$/+, *Nox3*^{het}/*Nox3*$^{het–2J}$, and +/+ genotypes on a fixed genetic background were assessed for VsEP threshold. *Nox3*^{het}/*Nox3*$^{het–2J}$ compound heterozygotes displayed no VsEP response, suggesting no residual function encoded by the *Nox3*$^{het–2J}$ allele. Moreover, *Nox3*$^{het–2J}$/+ mice retained the same VsEP threshold as their +/+ littermates, demonstrating that the *Nox3*$^{het–2J}$ allele has no antimorphic character acting to inhibit the wild-type allele.

With regard to the NOX3-interacting protein CYBA, the *Cyba*^{nmf333} allele encodes a nonconservative tyrosine-to-histidine substitution of amino acid 121 of the CYBA protein. *Cyba*^{nmf333}/*Cyba*^{nmf333} mutants display profound vestibular defects and have absent VsEP responses, and CYBA protein is not expressed in these mutants. Within phagocytic cells the absence of CYBA abolishes ROS generation, with the corresponding mice exhibiting a chronic granulomatous disease-like susceptibility to opportunistic infection (Nakano et al. 2008).

Summary

In sum, a number of mutant alleles exist for the NADPH oxidase components *Nox3*, *Noxo1*, and *Cyba*, with the corresponding mutant mouse strains showing profound vestibular dysfunction. The NOX3 protein, in particular, appears to be under strong constraint to conserve primary amino acid sequence as a variety of mutation types and locations tend to lead to a common loss-of-function phenotype. Identifying less severe alleles may require VsEP screening techniques to identify mice with elevated VsEP thresholds that may not show overt behavioral deficits.

Acknowledgments

The authors acknowledge the support of the Mouse Mutant Resource (NIH/NCRR grant RR001183) and the Computational Sciences Statistics and Analysis Group, Allele Typing & Sequencing Service, Fine Mapping

Laboratory, DNA Resource, and Cryopreservation Service of The Jackson Laboratory. The authors thank Ms. Leslie Haynes and The Jackson Laboratory Research Animal Facility staff for animal husbandry. The authors especially thank Dr. Yueming Ding for analysis of HTP sequence and Dr. Leah Rae Donahue, Director of the Genetic Resource Science group, for facilities and support. This work was supported by NIH/NIDCD grant DC007431 to DEB and NIH/NCI CORE grant CA34196 to JAX.

References

Banfi B, Malgrange B, Knisz J, Steger K, Dubois-Dauphin M, et al. NOX3, a superoxide-generating NADPH oxidase of the inner ear. J Biol Chem 2004;279:46065–46072. [PubMed: 15326186]

Bedard K, Krause KH. The NOX family of ROS-generating NADPH oxidases: physiology and pathophysiology. Physiol Rev 2007;87:245–313. [PubMed: 17237347]

Bergstrom, DE.; Bergstrom, RA.; Munroe, RJ.; Schimenti, JC.; Gagnon, LH., et al. The *Nox3* and *Noxo1* genes, encoding presumptive members of an NADPH oxidase complex, are required for normal vestibular function and development; 18th international mammalian genome conference; Seattle, WA. 17–22 Oct 2004; 2004.

Burke B, Stewart CL. The laminopathies: the functional architecture of the nucleus and its contribution to disease. Annu Rev Genomics Hum Genet 2006;7:369–405. [PubMed: 16824021]

Capell BC, Collins FS. Human laminopathies: nuclei gone genetically awry. Nat Rev Genet 2006;7:940–952. [PubMed: 17139325]

Cheng G, Cao Z, Xu X, van Meir EG, Lambeth JD. Homologs of gp91phox: cloning and tissue expression of *Nox3*, *Nox4*, and *Nox5*. Gene 2001;269:131–140. [PubMed: 11376945]

Darrat I, Ahmad N, Seidman K, Seidman MD. Auditory research involving antioxidants. Curr Opin Otolaryngol Head Neck Surg 2007;15:358–363. [PubMed: 17823554]

Goldowitz D, Frankel WN, Takahashi JS, Holtz-Vitaterna M, Bult C, et al. Large-scale mutagenesis of the mouse to understand the genetic bases of nervous system structure and function. Brain Res Mol Brain Res 2004;132:105–115. [PubMed: 15582151]

Guthrie OW. Aminoglycoside induced ototoxicity. Toxicology 2008;249:91–96. [PubMed: 18514377]

Henderson D, McFadden SL, Liu CC, Hight N, Zheng XY. The role of antioxidants in protection from impulse noise. Ann N Y Acad Sci 1999;884:368–380. [PubMed: 10842607]

Henderson D, Bielefeld EC, Harris KC, Hu BH. The role of oxidative stress in noise-induced hearing loss. Ear Hear 2006;27:1–19. [PubMed: 16446561]

Hosokawa M. A higher oxidative status accelerates senescence and aggravates age-dependent disorders in SAMP strains of mice. Mech Ageing Dev 2002;123:1553–1561. [PubMed: 12470893]

Jones TA, Jones SM. Short latency compound action potentials from mammalian gravity receptor organs. Hear Res 1999;136:75–85. [PubMed: 10511626]

Jones SM, Erway LC, Bergstrom RA, Schimenti JC, Jones TA. Vestibular responses to linear acceleration are absent in otoconia-deficient C57BL/6JEi-het mice. Hear Res 1999;135:56–60. [PubMed: 10491954]

Jones SM, Subramanian G, Avniel W, Guo Y, Burkard RF, et al. Stimulus and recording variables and their effects on mammalian vestibular evoked potentials. J Neurosci Methods 2002;118:23–31. [PubMed: 12191754]

Jones SM, Johnson KR, Yu H, Erway LC, Alagramam KN, et al. A survey of vestibular function in mutant mouse strains. Assoc Res Otolaryngol. 2003a abstract.

Jones SM, Johnson KR, Yu H, Zheng QY, Erway LC, et al. A comparison of vestibular and auditory function in inbred mouse strains. Assoc Res Otolaryngol. 2003b abstract.

Jones SM, Erway LC, Johnson KR, Yu H, Jones TA. Gravity receptor function in mice with graded otoconial deficiencies. Hear Res 2004;191:34–40. [PubMed: 15109702]

Jones SM, Johnson KR, Yu H, Erway LC, Alagramam KN, et al. A quantitative survey of gravity receptor function in mutant mouse strains. J Assoc Res Otolaryngol 2005;6:297–310. [PubMed: 16235133]

Jones SM, Jones TA, Johnson KR, Yu H, Erway LC, et al. A comparison of vestibular and auditory phenotypes in inbred mouse strains. Brain Res 2006;1091:40–46. [PubMed: 16499890]

Jurka J, Kapitonov VV, Pavlicek A, Klonowski P, Kohany O, et al. Repbase update, a database of eukaryotic repetitive elements. Cytogenet Genome Res 2005;110:462–467. [PubMed: 16093699]

Kent WJ, Sugnet CW, Furey TS, Roskin KM, Pringle TH, et al. The human genome browser at UCSC. Genome Res 2002;12:996–1006. [PubMed: 12045153]

Kiss PJ, Knisz J, Zhang Y, Baltrusaitis J, Sigmund CD, et al. Inactivation of NADPH oxidase organizer 1 results in severe imbalance. Curr Biol 2006;16:208–213. [PubMed: 16431374]

Klungland A, Laake K, Hoff E, Seeberg E. Spectrum of mutations induced by methyl and ethyl methanesulfonate at the *hprt* locus of normal and tag expressing Chinese hamster fibroblasts. Carcinogenesis 1995;16:1281–1285. [PubMed: 7788844]

Kopke R, Allen KA, Henderson D, Hoffer M, Frenz D, et al. A radical demise. Toxins and trauma share common pathways in hair cell death. Ann N Y Acad Sci 1999;884:171–191. [PubMed: 10842593]

Li H, Durbin R. Fast and accurate long-read alignment with Burrows–Wheeler transform. Bioinformatics 2010;26:589–595. [PubMed: 20080505]

Mouse Mutant Resource Web Site. Mouse mutant resource web site. The Jackson Laboratory; Bar Harbor, ME: 2010.

Mukherjea D, Jajoo S, Kaur T, Sheehan KE, Ramkumar V, et al. Transtympanic administration of short interfering (si)RNA for the NOX3 isoform of NADPH oxidase protects against cisplatin-induced hearing loss in the rat. Antioxid Redox Signal 2010;13:589–598. [PubMed: 20214492]

Munroe RJ, Bergstrom RA, Zheng QY, Libby B, Smith R, et al. Mouse mutants from chemically mutagenized embryonic stem cells. Nat Genet 2000;24:318–321. [PubMed: 10700192]

Nakano Y, Banfi B, Jesaitis AJ, Dinauer MC, Allen LA, et al. Critical roles for p22phox in the structural maturation and subcellular targeting of Nox3. Biochem J 2007;403:97–108. [PubMed: 17140397]

Nakano Y, Longo-Guess CM, Bergstrom DE, Nauseef WM, Jones SM, et al. Mutation of the *Cyba* gene encoding p22phox causes vestibular and immune defects in mice. J Clin Invest 2008;118:1176–1185. [PubMed: 18292807]

Paffenholz R, Bergstrom RA, Pasutto F, Wabnitz P, Munroe RJ, et al. Vestibular defects in head-tilt mice result from mutations in *Nox3*, encoding an NADPH oxidase. Genes Dev 2004;18:486–491. [PubMed: 15014044]

Rozen S, Skaletsky H. Primer3 on the WWW for general users and for biologist programmers. Methods Mol Biol 2000;132:365–386. [PubMed: 10547847]

Rybak LP, Whitworth CA, Mukherjea D, Ramkumar V. Mechanisms of cisplatin-induced ototoxicity and prevention. Hear Res 2007;226:157–167. [PubMed: 17113254]

Scharner J, Gnocchi VF, Ellis JA, Zammit PS. Genotype–phenotype correlations in laminopathies: how does fate translate? Biochem Soc Trans 2010;38:257–262. [PubMed: 20074070]

Stewart CL, Kozlov S, Fong LG, Young SG. Mouse models of the laminopathies. Exp Cell Res 2007;313:2144–2156. [PubMed: 17493612]

Sweet H. Head tilt. Mouse News Lett 1980;63:19.

van den Berg JH, Beijnen JH, Balm AJ, Schellens JH. Future opportunities in preventing cisplatin induced ototoxicity. Cancer Treat Rev 2006;32:390–397. [PubMed: 16781082]

Worman HJ, Fong LG, Muchir A, Young SG. Laminopathies and the long strange trip from basic cell biology to therapy. J Clin Invest 2009;119:1825–1836. [PubMed: 19587457]

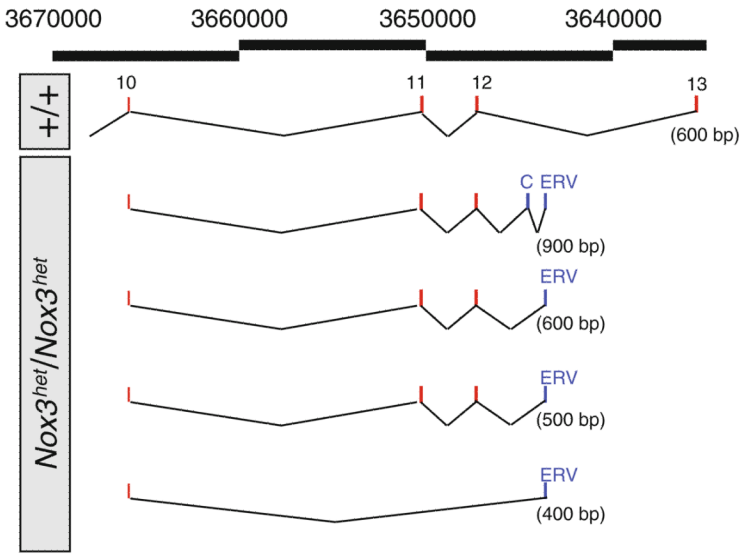

Fig. 1.

3′ RACE analysis of *Nox3*^{het} transcripts. 3′ RACE analysis of *Nox3*^{het}/*Nox3*^{het} inner-ear total RNA reveals the aberrant splicing products shown here that terminate in a sequence showing similarity to the sequences of mouse endogenous retroviruses. Alternating *black lines* with numbers, genome coordinates on Chromosome 17 (build 37); top schematic, 3′ RACE products from wild-type RNA; remaining schematics, 3′ RACE products from mutant RNA that splice into an exon derived from the endogenous retroviral sequence (ERV), may include a cryptic exon (C) or may skip exons 11 and 12. The size difference observed between the second and third mutants' 3′ RACE products is due to a difference in the size of included ERV sequence

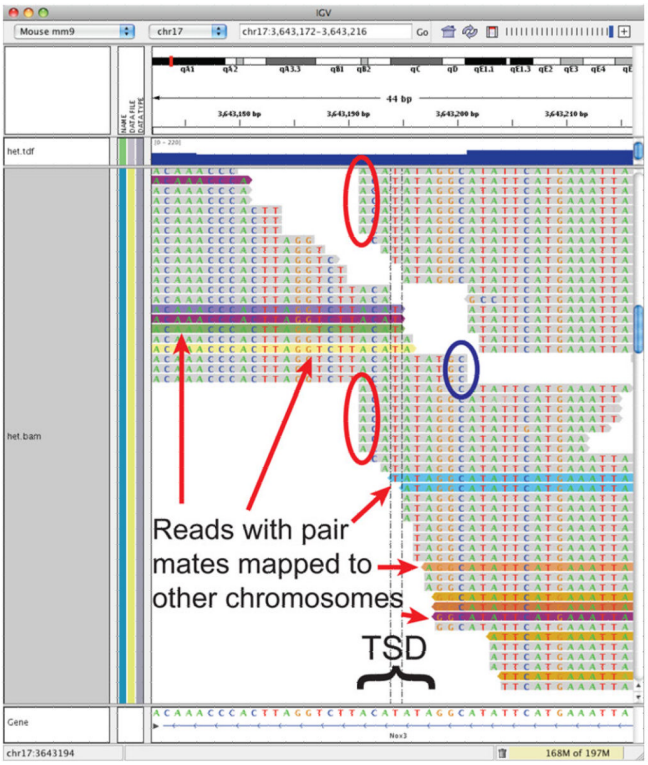

Fig. 2.

Integrative genome viewer (IGV) display of the endogenous retroviral insertion site in the *Nox3*^{het} allele. The IGV display of the endogenous retroviral insertion site reveals signatures indicative of the insertion, including truncation of reads directed distally (*red ovals*), truncation of reads directed proximally (*blue oval*), reads with pair mates mapped to other chromosomes (*variously colored reads*), and overlap of truncated reads in the area of an ACATATA target site duplication (TSD)

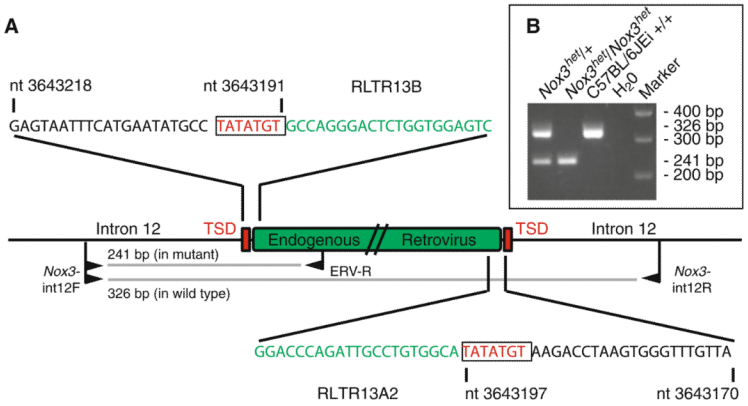

Fig. 3.

Detailed description of the endogenous retroviral insertion site in the *Nox3*^{het} allele. **a** Schematic describing the endogenous retroviral (ERV) insertion in the *Nox3*^{het} allele. *Central horizontal line*, intron 12 of the *Nox3* gene; *green rectangle*, ERV; *red rectangles*, target site duplications (TSD); *black sequences*, partial sequence from intron 12; *red sequences*, target site duplication; *green sequences*, partial ERV sequences showing similarity to ERV classes RLTR13B and RLTR13A2; nucleotide (*nt*) numbers, Chromosome 17 genome positions (build 37); *black flags*, PCR primers; *gray lines*, amplification products from the wild-type and mutant alleles. **b** (*inset*) The *Nox3*^{het} genotyping assay detects a 326-bp fragment in wild-type mice, a 241-bp fragment in *Nox3*^{het} mutant mice, and both fragments in heterozygous mice

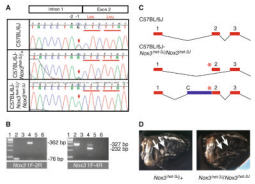

Fig. 4.

Analysis of the *Nox3*$^{het–3J}$ allele. **a** Sanger sequencing-based confirmation of the *Nox3*$^{het–3J}$ mutation identified by HTP sequencing. The mutation consists of a G > A transition at the −1 position of the splice acceptor site just prior to exon 2. **b** RT-PCR analysis of C57BL/6J and *Nox3*$^{het–3J}$/*Nox3*$^{het–3J}$ inner-ear RNA with 1F/2R and 1F/4R primer pairs. *Lane 1*, 100-bp ladder; *lane* 2, wild-type RNA; *lane 3*, negative reverse transcriptase (−RT) control; *lane 4*, *Nox3*$^{het–3J}$/*Nox3*$^{het–3J}$ RNA; *lane* 5, −RT control; *lane* 6, no template control. **c** Models of wild-type (C57BL/6J) and mutant (C57BL/6J-*Nox3*$^{het–3J}$/*Nox3*$^{het–3J}$) *Nox3* transcripts. *Red numbered rectangles*, exons; *asterisk*, mutation; C, cryptic splice acceptor; *blue rectangle*, intronic sequence incorporated into the mutant transcript. **d** Whole-mount preparation of cleared temporal bones from adult *Nox3*$^{het–3J}$/+ and *Nox3*$^{het–3J}$/*Nox3*$^{het–3J}$ mice. Note the presence of otoconia (*arrows*) in the heterozygotes and their absence in mutant homozygotes

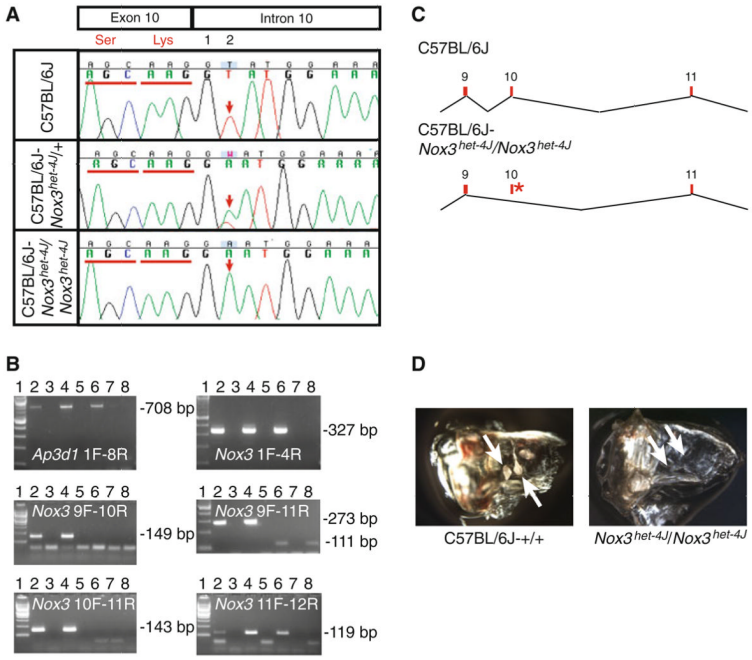

Fig. 5.

Analysis of the *Nox3*$^{het–4J}$ allele. **a** Sanger sequencing-based identification of the *Nox3*$^{het–4J}$ mutation. The mutation consists of a T > A transversion at the +2 position of the splice donor site just after exon 10. **b** RT-PCR analysis of C57BL/6J and *Nox3*$^{het–4J}$/*Nox3*$^{het–4J}$ inner-ear RNA with *Ap3d1* 1F/8R (positive control) primers as well as the *Nox3* 1F/4R, 9F/10R, 9F/11R, 10F/11R, and 11F/12R primer pairs. *Lane 1*, 100-bp ladder; *lane 2*, wild-type RNA; *lane 3*, negative reverse transcriptase (−RT) control; *lane 4*, *Nox3*$^{het–4J}$/+ RNA; *lane 5*, −RT control; *lane 6*, *Nox3*$^{het–4J}$/*Nox3*$^{het–4J}$ RNA; *lane 7*, −RT control; *lane 8*, no template control. **c** Models of wild-type (C57BL/6J) and mutant (C57BL/6J-*Nox3*$^{het–4J}$/*Nox3*$^{het–4J}$) *Nox3* transcripts. *Red numbered rectangles*, exons; *asterisk*, mutation. **d** Whole-mount preparation of cleared temporal bones from adult C57BL/6J-+/+and *Nox3*$^{het–4J}$/*Nox3*$^{het–4J}$ mice. Note the presence of otoconia (*arrows*) in the wild-type preparation and their absence in mutant homozygotes

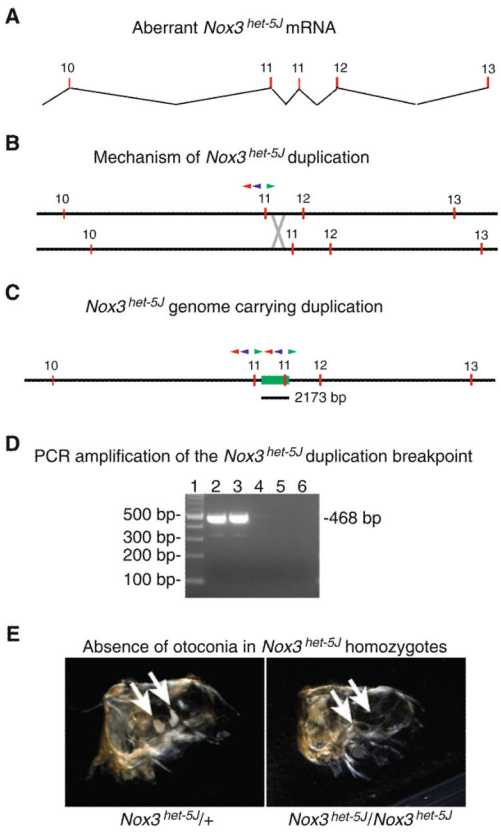

Fig. 6.

Analysis of the *Nox3*$^{het–5J}$ allele. **a** RT-PCR analysis and Sanger sequencing identified a duplication of exon 11 in *Nox3*$^{het–5J}$ cDNA. *Numbered red rectangles*, exons. **b** Proposed mechanism for the *Nox3*$^{het–5J}$ duplication by uneven crossing over. *Numbered red rectangles*, exons; *red triangle*, *Nox3*-44516R primer; *blue triangle*, *het-5J*R primer; *green triangle*, *Nox3*-46393F primer; *gray* X, crossover event. **c** Schematic of the *Nox3*$^{het–5J}$ allele. *Red numbered rectangles*, exons; *green rectangle*, duplicated region of 2173 bp encompassing exon 11; *red*, *blue*, and *green triangles* are as in **b**. Note that in the duplication-bearing allele, the three primers located between exons 11 are now pointed toward each and are able to support amplification. **d** Amplification across the duplication in the *Nox3*$^{het–5J}$ allele with the *Nox3*-46393F and *het-5J*R primers. *Lane 1*, 100-bp ladder; *lanes 2–3*, *Nox3*$^{het–5J}$/*Nox3*$^{het–5J}$ DNA; *lanes 4–5*, wild-type DNA; *lane 6*, no template control. **e** Whole-mount preparation of cleared temporal bones from adult *Nox3*$^{het–5J}$/+ and *Nox3*$^{het–5J}$/*Nox3*$^{het–5J}$ mice. Note the presence of otoconia (*arrows*) in the heterozygotes and their absence in mutant homozygotes

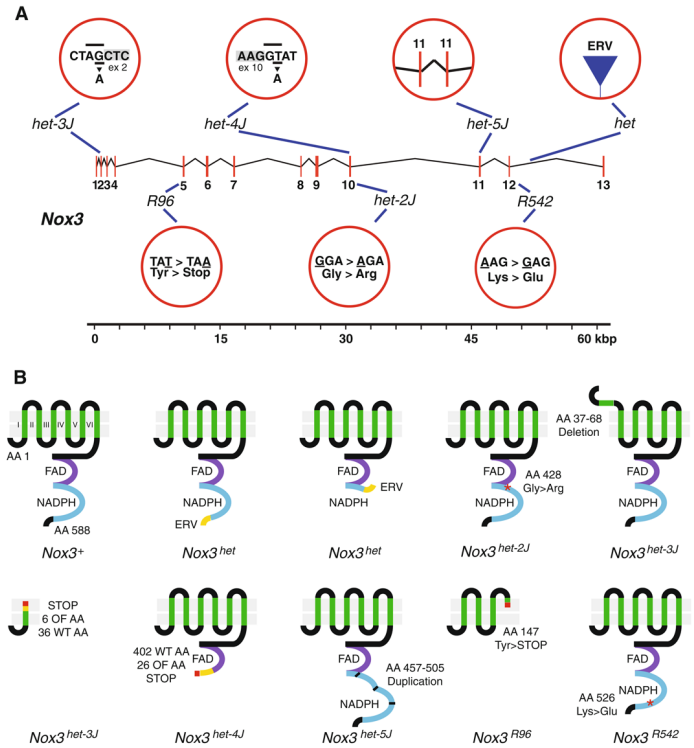

Fig. 7.

A summary of the mutations in *Nox3* and their effects on the NOX3 protein. **a** Shown are the *Nox3* transcription unit (*numbered vertical red lines*, exons) as well as the mutations occurring in the *het*, *het-2J*, *het-3J*, *het-4J*, *het-5J*, *R96*, and *R542* alleles of *Nox3*. For the *het* allele: *ERV* endogenous retrovirus. For the *het-2J*, *R96*, and *R542* alleles: shown are the wild-type (*left*) and mutant (*right*) codons and amino acids. The nucleotide that underwent mutation is underlined. For the *het-3J* and *het-4J* alleles: shown are seven nucleotides at the intron/exon boundary. *Gray labeled rectangle*, exon; *underlined*, wild-type nucleotide with mutant nucleotide shown below; *overlined*, AG/GT splicing acceptor/donor dinucleotide sequence. For the *het-5J* allele: shown are the duplicated exons 11. Also shown is a 60-kbp scale. **b** Shown schematically are the predicted effects of *Nox3* mutant alleles on the NOX3 protein. *Numbered green vertical lines*, transmembrane domains; *purple lines*, FAD binding domains; *blue lines*, NADPH binding domains; *yellow lines*, novel amino acids encoded by the endogenous retrovirus (*het*) or due to frameshift mutations (*het-3J* and *het-4J*); *red asterisks*, missense mutations; shortened first transmembrane domain in *het-3J*, in-frame deletion; *red lines*, premature stop codons; segmented *blue line* in *het-5J*, in-frame duplication of the second region of the NADPH binding domain; *AA* amino acid, *ERV* endogenous retrovirus, *FAD*, FAD binding domain; *NADPH*, NADPH binding domain; *OF* out-of-frame, *WT* wild type. This figure is a schematic representation of the effects of *Nox3* mutant alleles on translation and is not meant to imply that mutant proteins are present or properly targeted to the cell membrane

Table 1

Oligonucleotides

Nox3^{het}	
Genotyping	
Nox3-int12F	GTTCTGGAGCACCACCTTGT (use at 200 nM)
Nox3-int12R	CCCATAGGGAGCCAAGAAAT (use at 300 nM)
ERV-R	TGTCAAGCTGACTCCACCAG (use at 100 nM)
RACE	
3′RACE outer primer	GCGAGCACAGAATTAATACGACT
3′RACE inner primer	CGCGGATCCGAATTAATACGACTCACTATAGG
3′*Nox*InH	CGCAAGCTTTATTTCACTACCCCGTGAGC
3′*Nox*Out	CATGCCGAGGCTAGCAGT
3′RaceInX (3′ RACE adapter)	CGCCTCGAGGAATTAAATACGACTCACTATAGGT$_{12}$VN
Nox3$^{het–2J}$	
Genotyping	
Nox3-10F	GGCAGAGGAGAGATTTGAGG
Nox3-10R	TGGGATGTCTTTGTGTCCAA
Nox3$^{het–3J}$	
Genotyping	
Nox3-673F	TGACAACTTCTGCATTTCATCTG
Nox3-939R	GGAGGATGATGAAAACATTGAAG
RT-PCR	
*Nox3*ex-1F	TGTCATGCCGGTGTGCTGGA
*Nox3*ex-2R	AGGCGTTTACTGCCAGCCAT
*Nox3*ex-4R	CCCGTAGGCAACGAGTTTGTGGA
Nox3$^{het–4J}$	
Genotyping	
Nox3-10F	GGCAGAGGAGAGATTTGAGG
Nox3-10R	TGGGATGTCTTTGTGTCCAA
RT-PCR	
*Ap3d1*ex-1F	TCCGCAACCACAAGGAGGACGA
*Ap3d1*ex-8R	TCGATCAGCTTCTTGCCCAGCC
*Nox3*ex-1F	TGTCATGCCGGTGTGCTGGA
*Nox3*ex-4R	CCCGTAGGCAACGAGTTTGTGGA
*Nox3*ex-9F	TCAGGAGACTGGACAGAGGCGT
*Nox3*ex-10F	ACCCCGTGAGCGTGTGCATT
*Nox3*ex-10R	AATGCACACGCTCACGGGGT
*Nox3*ex-11F	CTCACTGGCTGGGATGAAAACCA
*Nox3*ex-11R	CGGCATCCCGGCAGATCCAATA
*Nox3*ex-12R	TTCGTCGTTCCAGTTGGGTCGC
Nox3$^{het–5J}$	
Amplification of duplication breakpoint	

Nox3-46393F	CCGAGGATCTCCATTACTGC
Nox3-44516R	GCAGATACCAAATTGCACTCTG
*het-5J*R	AAGACGTCTCCCATGTTCCA
Nox3^{R96}	
Genotyping	
*Nox3*R96-F	GCATTTGGCAGAAACCTCTT
*Nox3*R96-R	CACTGGGAGAGATGCACAAA
Nox3^{R542}	
Genotyping	
*Nox3*R542-F	AATAAAGCATTTCAAGCCGTG
*Nox3*R542-R	TTGTCTGGACTTCAGGGAGG

The oligonucleotides shown here are those used for the genotyping, RACE, RT-PCR, and duplication breakpoint analyses of *Nox3*^{het}, *Nox3*$^{het–3J}$, *Nox3*$^{het–4J}$, and *Nox3*$^{het–5J}$ alleles described in the text. Although the molecular lesions of the *Nox3*$^{het–2J}$, *Nox3*^{R96}, and *Nox3*^{R542} alleles have been described elsewhere, genotyping primers are provided here for the detection of those alleles. A *Hin*dIII site (in the 3′*Nox*InH oligonucleotide) and an *XhoI* site (in the 3′RaceInX oligonucleotide) that were used for cloning the 3′ RACE product from the *Nox3*^{het} allele are *underlined*. Primer names and numbering are arbitrary

Table 2

Mutant alleles[a] of the inner ear's NADPH oxidase components *Cyba*, *Noxol*, and *Nox3*

Gene	Allele	Strain of origin (current strain)	Mutation	Documented phenotypes	Effect to transcript/protein	Reference
Cyba	*nmf333*	A.B6->Tyr^{+}/J (same)	ENU-induced T > C transition in exon 5	B, O, V	Tyr > His; nonconservative substitution; no protein expression; no haploinsufficiency observed	Nakano et al. 2008
Noxol	*hslt*	*SJL/l-Thy1*^{a}*/J* (SJL/J)	Spontaneous A insertion in exon 1	B, O, V	Frameshift; premature stop; transcript is detectable; haploinsufficiency observed	Bergstrom et al. 2004; Kiss et al. 2006; K.N. Mills and S.M. Jones, personal communication
Nox3	*het*	GL/Le (B6ELGL congenic)	Spontaneous ERV insertion in intron 12 (see text)	B, O, V	Splicing abnormalities; transcript is detectable	Paffenholz et al. 2004; and this report
	het-2J	B10.D1-*H2*^{q}/SgJ (B6 × B10.D1-*H2*^{q}/SgJ hybrid)	Spontaneous G > A transition in exon 10	B, O, V[b]	Gly > Arg; nonconservative substitution; not hypermorphic or antimorphic	Paffenholz et al. 2004; K.N. Mills and S.M. Jones, personal communication
	het-3J	129S1/SvImJ (B6.129S1 congenic)	EMS-induced G > A transition at splice acceptor in intron 1 (see text)	B, O	Skipping of exon 2 with no frameshift; deletion of first transmembrane domain; use of cryptic splice acceptor in intron 1 with frameshift and premature stop	This report
	het-4J	C57BL/6J (same)	ENU-induced T > A transversion at splice donor in intron 10 (see text)	B, O, V	Skipping of exon 10 with frameshift and premature stop	This report and K.N. Mills and S.M. Jones, personal communication
	het-5J	CBySmn.CB17-*Prkdc*^{scid}/J (BALB/cByJ)	Spontaneous tandem duplication encompassing exon 11 (see text)	B, O	Duplication of amino acids 457–505 of the NADPH binding domain	This report
	R96	C3HeB/FeJ (same)	ENU-induced T > A transversion in exon 5	B, O	Tyr > premature stop	Paffenholz et al. 2004
	R542	C3HeB/FeJ (same)	ENU-induced A > G transition in exon 12	B, O	Lys > Glu; nonconservative substitution	Paffenholz et al. 2004

The known spontaneously arising and mutagen-induced mutant alleles of *Cyba*, *Noxo1*, and *Nox3* are shown along with strain information, the nature of the mutation, documented phenotypes, and the known or predicted effect on transcript/protein expression

B behavioral, *O* absence of otoconia, *V* absence of VsEPs

[a] In addition to the alleles shown, there are a number of curated gene-trapped and gene-targeted alleles of *Nox3*, *Noxo1*, and *Cyba* represented only as cell lines. At the time of this writing, none of these lines has been used to create mice and therefore no vestibular phenotype information is available for these lines. Furthermore, the characterization of these gene-trapped and genetargeted cell lines is well understood as they have been designed, a *priori*, to create null alleles of the altered genes

[b] VsEPs are absent in *Nox3*^{het}/*Nox3*$^{het–2J}$ compound heterozygotes